Geochemical Perspectives Letters

In situ redox control and Raman spectroscopic characterisation of solutions below 300 °C

I.-M. Chou, R. Wang, J. Fang

Supplementary Information

The Supplementary Information includes:

- S-1. Previous Redox Buffer Techniques Without Precious Metal Hydrogen Membranes
- S-2. Optical Cell Setup and Sample Preparation
- S-3. Collection and Processing of Raman Spectra
- S-4. Temperature Effect on the Sn-Cl Complexes in a Vapour-saturated Sn-H-Cl Aqueous Solution
- S-5. Deconvolution of Raman Bands of $Sn^{II\ \&\ IV}$-Cl Complexes Collected at 30 °C Before and After Heating and Reduction
- S-6. The Presence of Unknown Sn^{IV} Species between 30 and 75 °C
- S-7. Reduction Kinetics of Sn^{IV}-Cl to Sn^{II}-Cl Complexes at 300 °C
- Figures S-1 to S-7
- Supplementary Information References

S-1. Previous Redox Buffer Techniques Without Precious Metal Hydrogen Membranes

To control the redox state of a sample in a hydrothermal experiment without using precious metal hydrogen membrane, many techniques have been applied, and they can be grouped into three categories (Fang and Chou, 2021): (1) loading a solid oxygen buffer together with studied samples without physical separation by a membrane (*e.g.*, Gibert *et al.*, 1998; Seewald, 2001; Tagirov *et al.*, 2005; Kokh *et al.*, 2017); (2) introducing a quartz tube oxygen buffer holder with one end sealed and the open end exposed to the vapour phase of the sample in an autoclave (*e.g.*, Archibald *et al.*, 2001; Timofeev *et al.*, 2018; Shang *et al.*, 2020); and (3) attaining internal redox equilibrium of multivalent species (*e.g.*, sulfur species) included in the studied system (*e.g.*, Pokrovski *et al.*, 2015; Kokh *et al.*, 2020).

S-2. Optical Cell Setup and Sample Preparation

A schematic diagram of the experimental setup is shown in Figure 1. A sample solution was loaded and sealed together with a vapour phase in an FSCC [150 μm inner diameter (ID), 375 μm outer diameter (OD) and ~ 6 mm long] following the procedures of Chou *et al.* (2008). This FSCC was then inserted in an HPOC (450 μm ID, 670 μm OD and ~17 cm long), which was then connected to a *P* line through a high-*P* valve (HiP 15-15AF1). The connected HPOC and *P* line were then vacuumed and flushed with H_2 (99.999 % from Guangdong Huate Gas Co.) three times before loading H_2, and its *P* was adjusted with a *P* generator and measured using a *P* transducer (25 psi in full scale and accurate to ±0.25 % of the full scale; Setra Systems, Inc.). The sample in the FSCC was heated to a fixed *T* on a heating-cooling stage (Linkam CAP500) and exposed to a fixed external P_{H_2} either during heating or after it reached the target *T*. The reported *T* has an accuracy of ±0.1 °C from 0 to 100 °C, which gradually increases to ±0.3 °C at 300 °C (Chen and Chou, 2020).

The used chemical reagents include $SnCl_4 \cdot 5H_2O$ crystals (98 %, Acros-Organics), hydrochloric acid (Analytical reagent, Xilong Scientific Co., Ltd.) and deionised H_2O (via a Millipore water filtration system; 18.24 MΩ·cm). A solution containing 0.5 *m* (mole/kg H_2O) $SnCl_4$ + 0.5 *m* HCl was then prepared and sealed in an FSCC, following the method of Chou *et al.* (2008), with the solution occupying approximately half of the available volume in the FSCC, such that the bulk density of the solution in the FSCC was approximately 0.5 g/ml and the solution was under vapour-saturation *P*s at experimental *T*s below 300 °C. Note that, in the preparation of the experimental system shown in Figure 2a, a short fused silica capillary tube with the same ID and OD as the FSCC, but with two ends open, was inserted in the HPOC (inner tube 2 in Fig. 2a). Because the intensity of a Raman band, such as the peak height, collected through two layers of fused silica will be lower than that collected through only one layer, therefore, it was necessary to insert inner tube 2 to yield the Raman signals of the external H_2 through two layers of fused silica, to be fairly compared with those collected from the FSCC.

S-3. Collection and Processing of Raman Spectra

A JY/Horiba LabRAM HR Evolution Raman spectrometer was applied to acquire the Raman spectra using a 532.06 nm (Nd: YAG) laser, a super-long-working-distance 50× Olympus objective with a 0.35 numerical aperture, and an 1800 groove/mm grating with a spectral resolution of approximately 0.65 cm^{-1}.

Approximately 14 mW of the laser light was focused near the center of the sample cell to generate the Raman signals during measurement. The peak heights of H_2 (PH_{H_2}) were calculated with an in-house program, similar to the GRAM32/AI software (used in Fang and Chou, 2021), and are available on request. Note that baseline removing process of spectra was done through the Labspec 5 software with a linear equation, and that a Peakfit 4.0 software and Gaussian-Lorentzian area function were used to deconvolute these spectroscopic bands. It was assumed that the quantities of Sn-Cl species were directly related to their peak areas.

S-4. Temperature Effect on the Sn-Cl Complexes in a Vapour-saturated Sn-H-Cl Aqueous Solution

To examine the *T* effect on the phase relations and Sn-Cl complexes in a vapour-saturated Sn-H-Cl aqueous solution, another FSCC was prepared from the same aqueous solution initially containing 0.5 *m* $SnCl_4$ and 0.5 *m* HCl. This FSCC was heated slowly, and many small particles were observed precipitating at ~125 °C (Fig. S-1a), which became larger in size and number at 300 °C (Fig. S-1b). This sample was cooled to 25 °C, and the precipitates were centrifuged to one end of the FSCC before being heated again to 300 °C (Fig. S-1c). The sample was kept at 300 °C for 3 hours, and crystals grew from these precipitates (Fig. S-1d), yielding the characteristic Raman peak of cassiterite at ~635 cm^{-1} (Scott, 1970; Fig. S-2). At this point, 0.2 bar of the external P_{H_2} was applied to the FSCC (Fig. S-1e). Cassiterite crystals could still be observed up to 56 hr (Figs. S-1f, g) but were not detected at 72 hr (Fig. S-1h). The *in situ* Raman spectra were then collected at 300 °C from the homogeneous fluid from time to time up to 311 hr under the vapour saturation *P*. The results (Fig. S-3) showed that about 276 hours are needed to reach the steady state distribution of Sn^{II} and Sn^{IV} species in the solution under the set P-T-P_{H_2} condition. It should be noted that the steady state was not reached at the reaction time of 156 hr (Fig. 3a, which is presented as a black dashed line in Fig. S-3). This sample was then quenched, and *in situ* Raman spectra were collected at various *T*s during heating from 30 to 300 °C under an externally imposed P_{H_2} of 0.2 bar, as shown in Figure 4. The spectrum was collected after the sample was kept at the specified *T* for at least 10 minutes. In our preliminary experiment, we found that the rates of conversions among $Sn^{II\ \&\ IV}$-Cl complexes in response to temperature change were fast (less than 5 min), which were much faster than those for reducing Sn^{IV}-Cl complexes to Sn^{II}-Cl complex under 0.2 bar of H_2. When the sample *T* was increased from 30 to 300 °C, the observed ~12 cm^{-1} low-wavenumber shift of Sn^{IV}-Cl complexes peak is in agreement with that reported by Schmidt (2018; Fig. 3 within the

paper). Note that the redox control was not ensured in Schmidt (2018), and that the presence of Sn^{II} in the study may be caused by the presence of contaminating H_2, which was produced by the reaction between diamond and H_2O catalyzed by the Ir gasket used in the study (see Fig. 1d and Table 1 of Chou and Anderson, 2009).

S-5. Deconvolution of Raman Bands of $Sn^{II\ \&\ IV}$-Cl Complexes Collected at 30 ˚C Before and After Heating and Reduction

Results of deconvolution of Raman spectroscopic bands of Sn^{IV}-Cl complexes collected at 30 ℃ from the second FSCC sample solution, initially containing 0.5 *m* $SnCl_4$ + 0.5 *m* HCl, under vapour-saturated pressure before further heating and H_2 exposure are shown in Figure S-4a, and those for $Sn^{II\ \&\ IV}$-Cl complexes after exposure to 0.2 bar of P_{H_2} at 300 ℃ for 311 hr (see Fig. S-3) are shown in Figure S-4b. Results show that the Sn^{IV}-Cl band was composed of 55 % $Sn^{IV}Cl_5(H_2O)^-$, 26 % $Sn^{IV}Cl_4(H_2O)_2^0$ and 19 % $Sn^{IV}Cl_3(H_2O)_3^+$ before heating and reduction (Fig. S-4a), and was changed to 24 %, 60 %, and 16 %, respectively, after heating and reduction (Fig. S-4b). These results imply that $Sn^{IV}Cl_5(H_2O)^-$ was possibly the main species being reduced in the initial solution at 300 °C under an externally imposed P_{H_2} of 0.2 bar.

S-6. The Presence of Unknown Sn^{IV} Species between 30 and 75 °C

A 3rd FSCC sample, containing 0.8 *m* $SnCl_4$ + 0.5 *m* HCl + 0.8 *m* NaCl solution and a vapour phase, was prepared for comparing Raman spectra collected during heating and cooling. During heating at the rate of 5 °C/min, cassiterite precipitated at about 125 °C, started to dissolve at about 225 °C, and was totally dissolved at 275 °C within one hour. After heating to 300 °C, the sample solution was then quickly quenched to 75 °C and slowly cooled down to 30 °C. No cassiterite was observed to precipitate during this cooling process, while a series of Raman spectra was collected. Figure S-5 shows that the intensities of Sn^{IV}-Cl complexes Raman bands collected during heating were obviously lower than those collected during cooling. Because there was no visible precipitation during the collection of these spectra, total Sn concentrations in all of these solutions remained the same. Therefore, at the same temperature (between 30 and 75 °C), the lower intensities of the Sn^{IV}-Cl complexes Raman bands collected during heating was possibly due to (1) the presence of unknown Sn^{IV} species, and (2) the slow decomposition rate of Sn^{IV}-Cl species at temperatures between 30 and 75 °C after they were formed at 300 °C.

S-7. Reduction Kinetics of Sn^{IV}-Cl to Sn^{II}-Cl Complexes at 300 °C

The reduction reaction of Sn^{IV}-Cl to Sn^{II}-Cl complexes at 300 °C under externally imposed P_{H_2} of 0.2 bar can be described by:

$$[Sn^{IV}Cl_n]^{4-n} + H_2 = [Sn^{II}Cl_3]^- + 2\,H^+ + (n-3)\,Cl^- \qquad \text{(Eq. S-1)}$$

where n = 3 to 6. According to Eq. S-1, the kinetic model rate equation of Sn^{IV}-Cl complexes reduction is expressed as:

$$-\frac{d[Sn^{IV}]}{dt} = k[Sn^{IV}][H_2] \qquad \text{(Eq. S-2)}$$

where k and t are the reaction rate constant and time, respectively, $[Sn^{IV}]$ is the total concentration of all Sn^{IV}-Cl complexes, including $Sn^{IV}Cl_6(H_2O)^{2-}$, $Sn^{IV}Cl_5(H_2O)^-$, $Sn^{IV}Cl_4(H_2O)_2^0$ and $Sn^{IV}Cl_3(H_2O)_3^+$, and $[H_2]$ is H_2 pressure. Because H_2 pressure was fixed at 0.2 bar during the reaction, therefore Eq. S-2 becomes:

$$-\frac{d[Sn^{IV}]}{dt} = k'[Sn^{IV}] \qquad \text{(Eq. S-3)}$$

where $k' = k[H_2] = 0.2\,k$.

Assuming that the initial total concentration of Sn^{IV}-Cl complexes is $[Sn^{IV}]_0$, and the total concentration of all Sn^{IV}-Cl complexes that have not been reduced in time t is $[Sn^{IV}]_t$, Eq. S-3 can be converted to :

$$\ln\frac{[Sn^{IV}]_0}{[Sn^{IV}]_t} = k't \qquad \text{(Eq. S-4)}$$

To minimize the instrumental effects of Raman system, Eq. S-4 is converted to:

$$\ln\frac{PAR_0}{PAR_t} = k't \qquad \text{(Eq. S-5)}$$

where PAR_0 and PAR_t are Raman peak area ratios between Sn^{IV}-Cl band and water band at time 0 and t, respectively. For example, Figure S-6 shows *PAR* for t = 0 and 229 hr, and the calculated data points are marked by red circles in Figure S-7, in which the slope of the black line represents the rate coefficient $\boldsymbol{k'}$. The rate coefficient $\boldsymbol{k'}$ of 0.0045 (h^{-1}) at 300 °C was obtained based on the data collected from the 2nd FSCC sample shown in Figure S-3. In the same manner, the rate coefficients $\boldsymbol{k'}$ calculated from the generated amount of Sn^{II}-Cl complex based on the *PAR* derived from $\nu_1[Sn^{II}Cl_3^-]$ band (~230 cm^{-1}) and $\nu_2[Sn^{II}Cl_3^-]$ band (~280 cm^{-1}) were 0.0046 and 0.0049 (h^{-1}), respectively, and they were in good agreement with 0.0045 (h^{-1}) derived from the Raman band of Sn^{IV}-Cl complexes described above.

Supplementary Figures

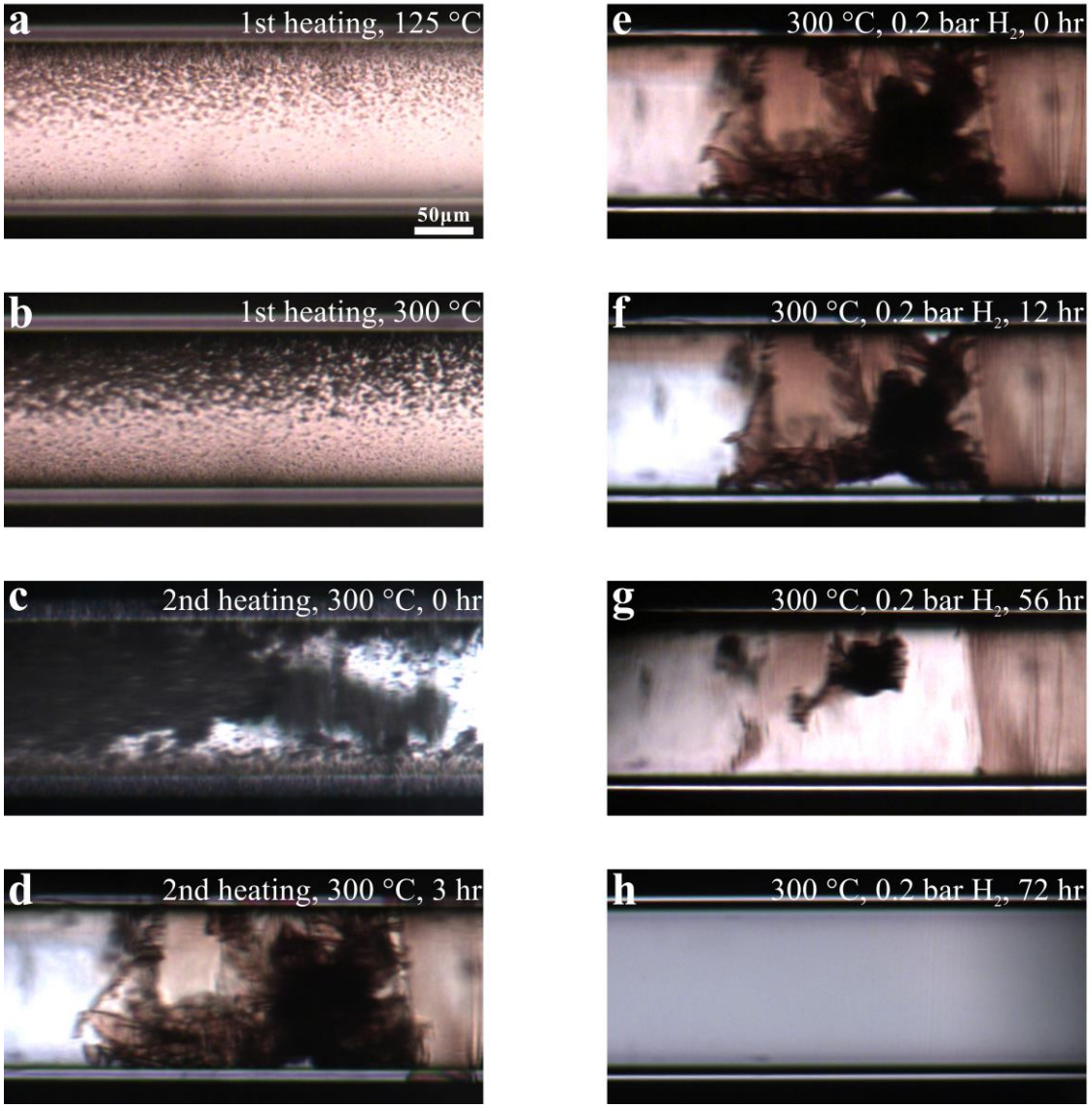

Figure S-1 Photomicrographs of an FSCC, initially containing 0.5 *m* $SnCl_4$ and 0.5 *m* HCl, taken at elevated *T*s under vapour-saturated *P*s without **(a-d)** and with **(e-h)** an externally imposed P_{H_2} of 0.2 bar. Initial precipitates were observed at approximately 125 °C **(a)**, and *in situ* Raman analysis of the crystals in **(d)** indicates that they were cassiterite (Fig. S-2), which could not be detected at 300 °C after being exposed to a P_{H_2} of 0.2 bar for 72 hours **(hr)**. For details, see the text. A scale bar is shown in **(a)**.

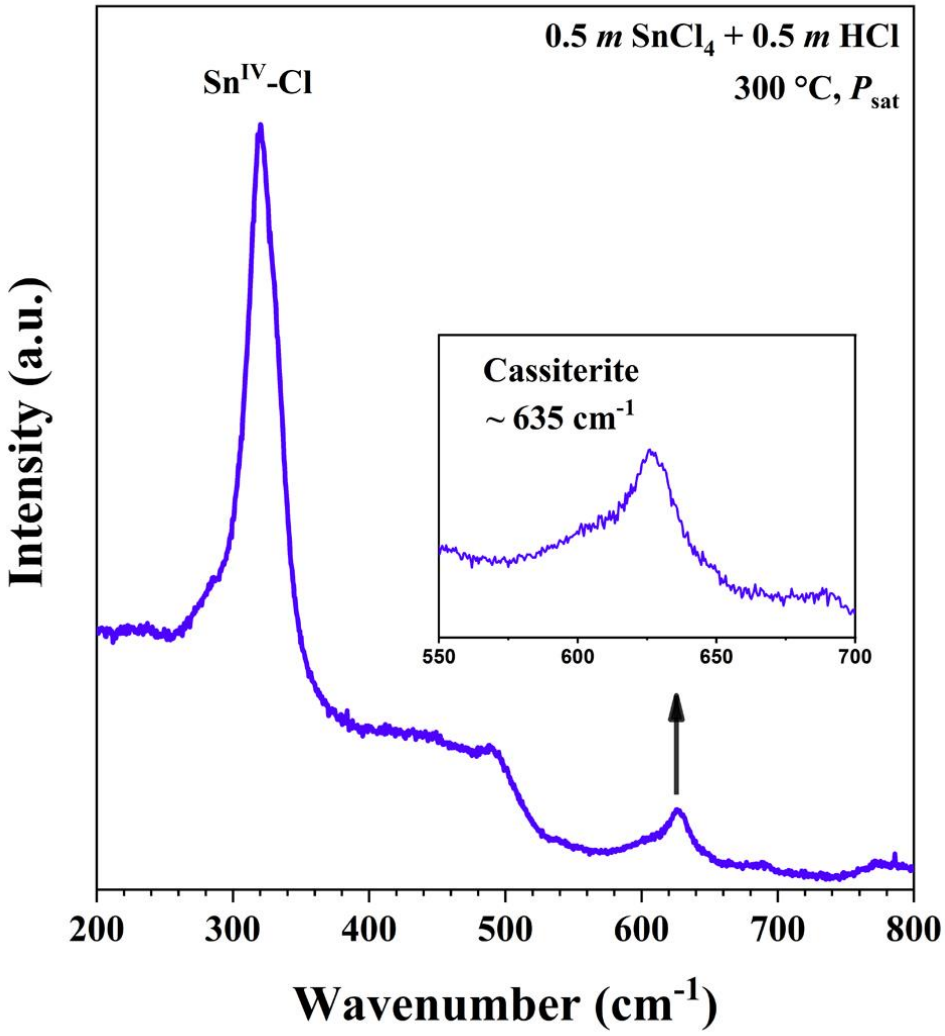

Figure S-2 *In situ* Raman spectrum collected from crystals shown in Figure S-1d. The insert shows the characteristic peak of cassiterite near 635 cm^{-1} (Scott, 1970). P_{sat} = vapour-saturated P.

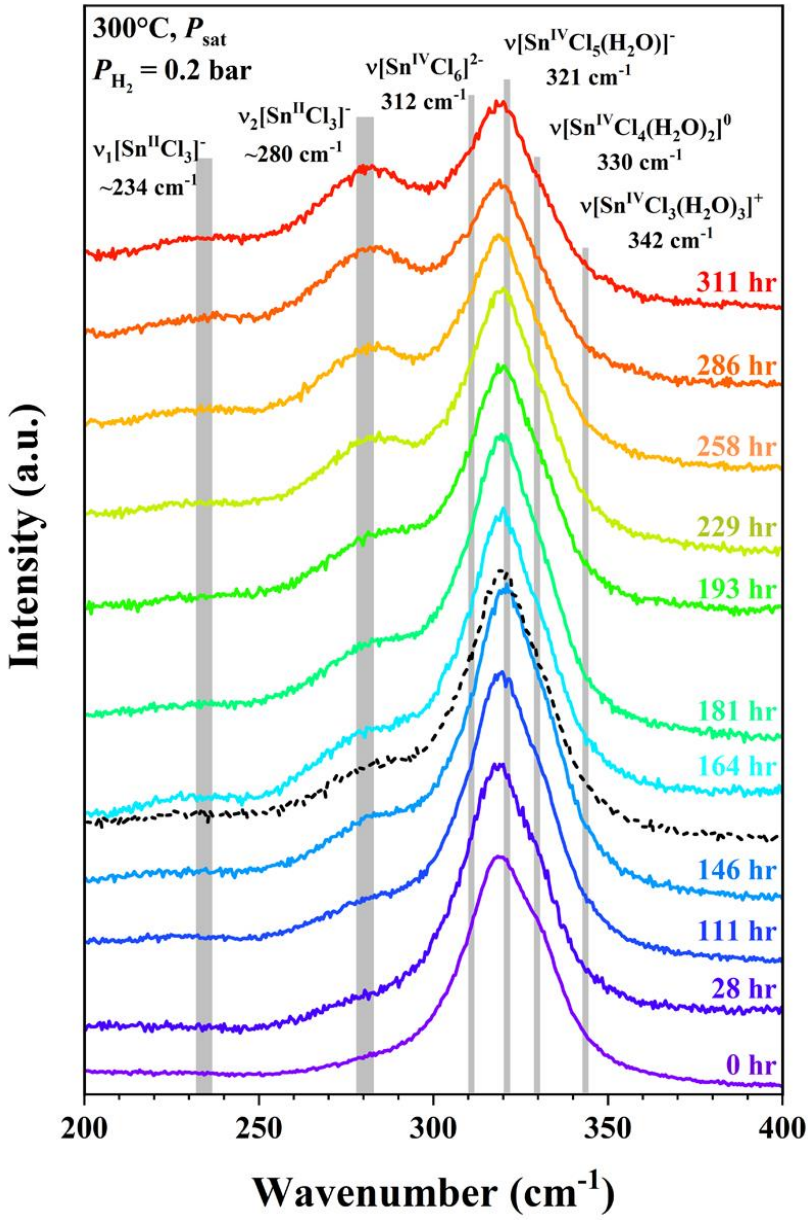

Figure S-3 *In situ* Raman spectra collected from the second FSCC sample (0.5 *m* $SnCl_4$ + 0.5 *m* HCl initial solution) at 300 °C under vapour-saturated *P* (P_{sat}) and an externally imposed P_{H_2} of 0.2 bar for durations up to 311 hours. For clarity, not all spectra are shown. For comparison, the spectrum collected at 156 hr shown in Figure 3a is presented here as the black dashed line, indicating that the system had not reached a steady state at that time. The vertical gray lines were taken from Schmidt (2018), showing Raman peak positions of various Sn-Cl species at ambient *P*-*T* conditions.

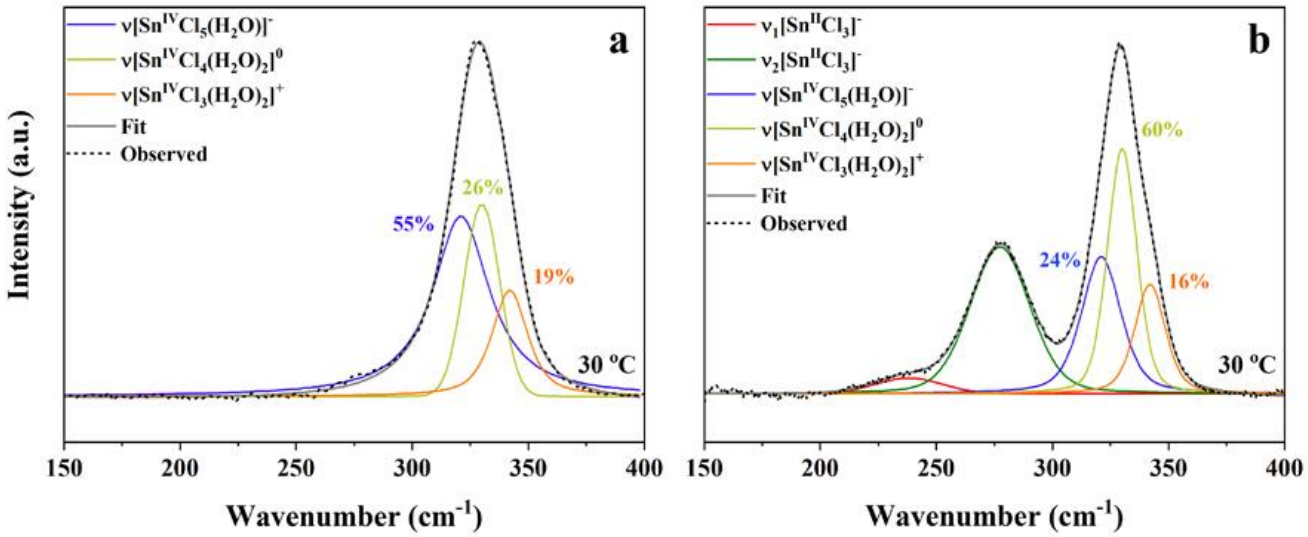

Figure S-4 Deconvolution of Raman bands of $Sn^{II\ \&\ IV}$-Cl complexes collected at 30 °C from the second FSCC sample solution initially containing 0.5 *m* $SnCl_4$ + 0.5 *m* HCl under vapour-saturated pressure (**a**) before further heating and H_2 exposure, and (**b**) after exposure to 0.2 bar of P_{H_2} at 300 °C for 311 hr (see Fig. S-3). No cassiterite precipitation was observed during the collection of both spectra. The marked percentages are for the Sn^{IV}-Cl complexes only.

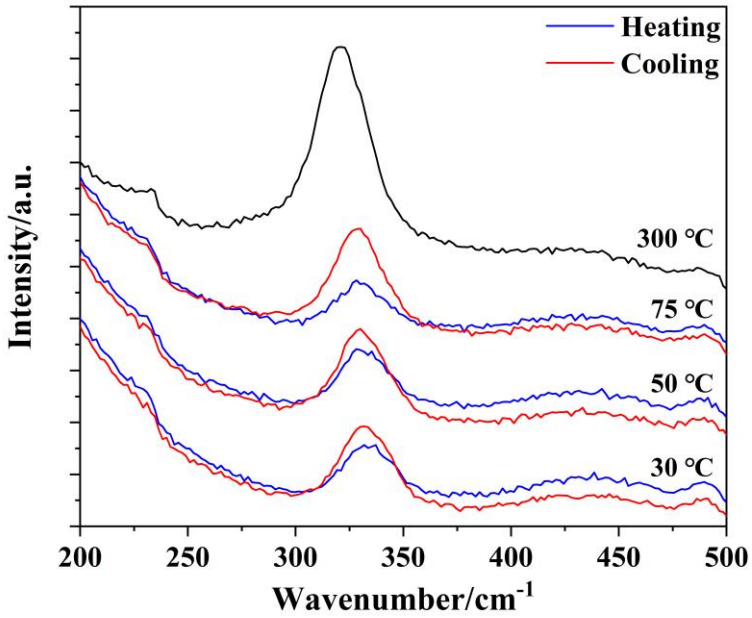

Figure S-5 Comparison of Raman bands of Sn^{IV}-Cl species collected from an aqueous solution in an FSCC containing 0.8 *m* $SnCl_4$ + 0.5 *m* HCl + 0.8 *m* NaCl during heating and cooling. Cassiterite precipitated at about 125 °C during heating (5 °C/min), then started to dissolve at about 225 °C and totally dissolved at 275 °C within one hour. There was no visible precipitation during the collection of all presented spectra. Raman intensities of the Sn^{IV}-Cl complex bands collected during heating (blue) were obviously lower than those collected during cooling (red), indicating the presence of unknown Sn^{IV} species.

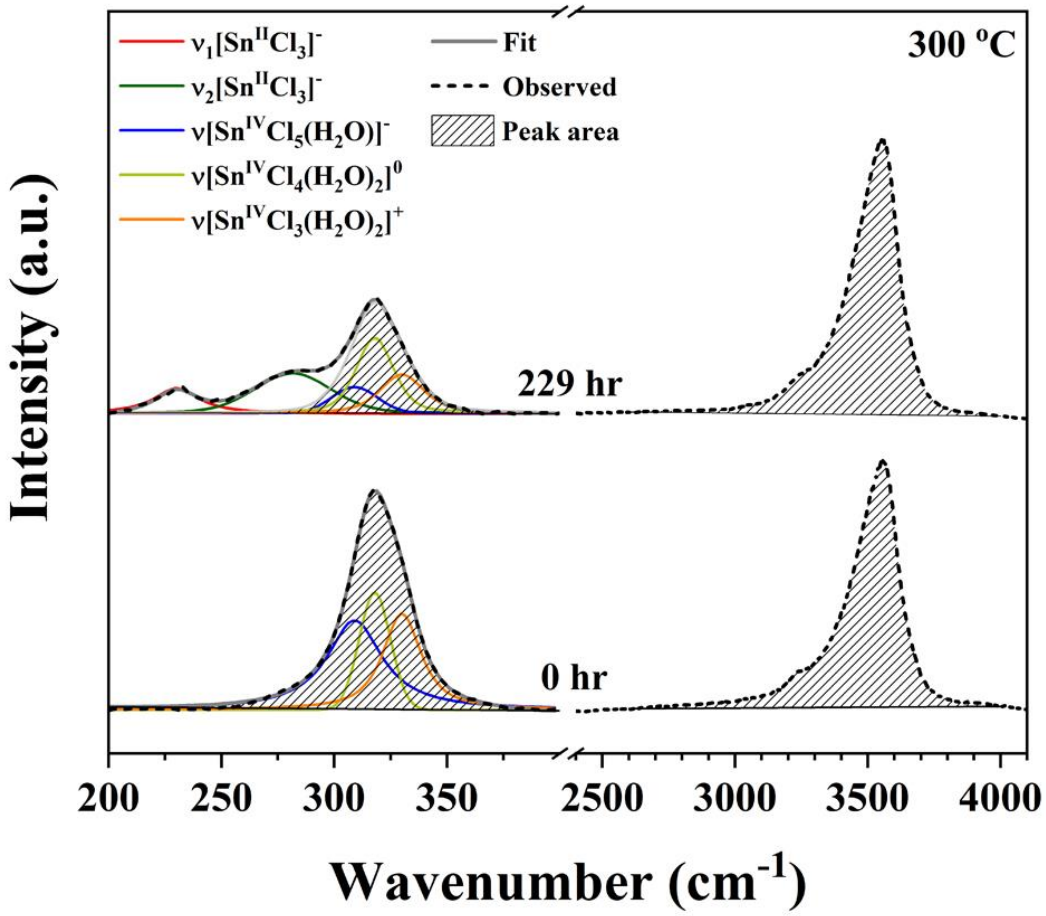

Figure S-6 Deconvolution of Raman spectroscopic bands of $Sn^{II\ \&\ IV}$-Cl complexes in two spectra collected from the second FSCC sample solution (initially containing 0.5 *m* $SnCl_4$ + 0.5 *m* HCl) at 300 °C under vapour-saturated *P* before (0 hr; lower spectrum below 400 cm^{-1}) and after being exposed to P_{H_2} of 0.2 bar for 229 hr (upper spectrum below 400 cm^{-1}). Also shown are the peak areas of Sn^{IV}-Cl complexes bands (ruled area below 400 cm^{-1}) together with those of H_2O band (ruled area between 2500 and 4000 cm^{-1}). The peak area ratios (*PAR*) between Sn^{IV}-Cl complexes band and H_2O band were calculated for time 0 and 229 hr and plotted in Figure S-7 (marked by red circles).

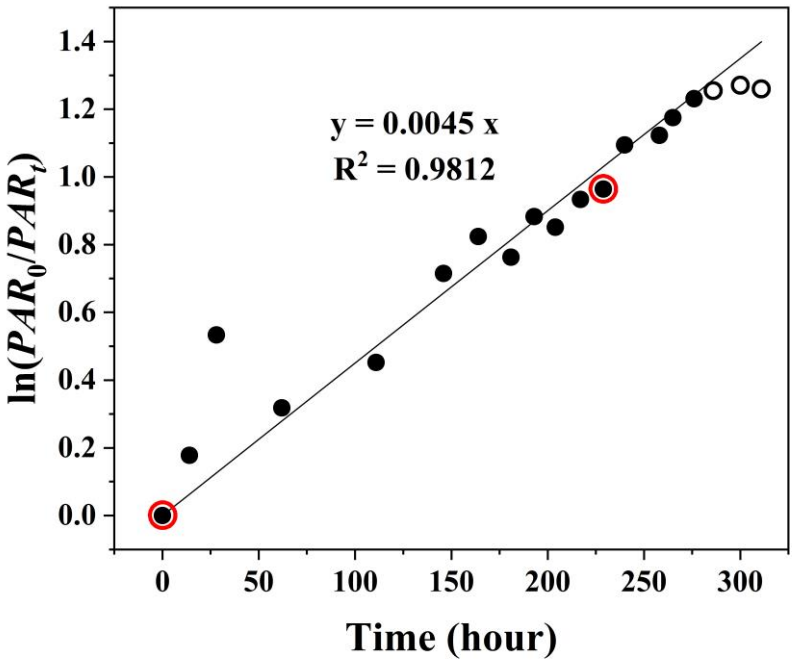

Figure S-7 Relationship between ln(PAR_0/PAR_t) and reaction time. Linear regression of the data shown by black dots yields the black line, the slop of which represents the rate coefficient, $\boldsymbol{k'}$. The three open black circles represent data points at 286, 300, and 311 hr; they were not included in linear regression as no further reduction was detected after 276 hr. The two data points enclosed by red circles were derived from Figure S-6 at 0 and 229 hr.

Supplementary Information References

Archibald, S.M., Migdisov, A.A., Williams-Jones, A.E. (2001) The stability of Au-chloride complexes in water vapor at elevated temperatures and pressures. *Geochimica et Cosmochimica Acta* 65, 4413–4423.

Chen, Y., Chou, I.M. (2020) Measurements of vapor pressures of aqueous solutions in the NaCl–KCl–H_2O system from 493.15 to 693.25 K in a fused silica capillary high-pressure optical cell. *Journal of Chemical & Engineering Data* 65, 766-776.

Chou, I.M., Anderson,A.J. (2009) Diamond dissolution and the production of methane and other carbon-bearing species in hydrothermal diamond-anvil cells. *Geochimica et Cosmochimica Acta* 73, 6360–6366.

Chou, I.M., Song, Y.C., Burruss, R.C. (2008) A new method for synthesizing fluid inclusions in fused silica capillaries containing organic and inorganic material. *Geochimica et Cosmochimica Acta* 72, 5217–5231.

Fang, J., Chou, I.M. (2021) Redox control and measurement in low-temperature (< 450 °C) hydrothermal experiments. *American Mineralogist* 106, 1333–1340.

Gibert, F., Pascal, M.L., Pichavant, M. (1998) Gold solubility and speciation in hydrothermal solutions: experimental study of the stability of hydrosulphide complex of gold (AuHS°) at 350 to 450°C and 500 bars. *Geochimica et Cosmochimica Acta* 62, 2931–2947.

Kokh, M.A., Akinfiev, N.N., Pokrovski, G.S., Salvi, S., Guillaume, D. (2017) The role of carbon dioxide in the transport and fractionation of metals by geological fluids. *Geochimica et Cosmochimica Acta* 197, 433–466.

Kokh, M.A., Assayag, N., Mounic, S., Cartigny, P., Gurenko, A., Pokrovski, G.S. (2020) Multiple sulfur isotope fractionation in hydrothermal systems in the presence of radical ions and molecular sulfur. *Geochimica et Cosmochimica Acta* 285, 100–128.

Pokrovski, G.S., Kokh, M.A., Guillaume, D., Borisova, A.Y., Gisquet, P., Hazemann, J.L., Lahera, E., Del Net, W., Proux, O., Testemale, D. (2015) Sulfur radical species form gold deposits on Earth. *Proceedings of the National Academy of Sciences* 112, 13484–13489.

Schmidt, C. (2018) Formation of hydrothermal tin deposits: Raman spectroscopic evidence for an important role of aqueous Sn(IV) species. *Geochimica et Cosmochimica Acta* 220, 499–511.

Scott, J. (1970) Raman spectrum of SnO_2. *Journal of Chemical Physics* 53, 852–853.

Seewald, J.S. (2001) Aqueous geochemistry of low molecular weight hydrocarbons at elevated temperatures and pressures: constraints from mineral buffered laboratory experiments. *Geochimica et Cosmochimica Acta* 65, 1641–1664.

Shang, L.B., Williams-Jones, A.E., Wang, X.S., Timofeev, A., Hu, R.Z., Bi, X.W. (2020) An experimental study of the solubiliy and speciation of MoO_3(s) in hydrothermal fluids at temperature up to 350°C. *Economic Geology* 115, 661–669.

Tagirov, B.R., Salvi, S., Schott, J., Baranova, N.N. (2005) Experimental study of gold-hydrosulphide complexing in aqueous solutions at 350–500°C, 500 and 1000 bars using mineral buffers. *Geochimica et Cosmochimica Acta* 69, 2119–2132.

Timofeev, A., Migdisov, A.A., Williams-Jones, A.E., Roback, R., Nelson, A.T., Xu, H. (2018) Uranium transport in acidic brines under reducing conditions. *Nature Communications* 9, 1–7.